EFFECT OF URBANIZATION ON LAND SURFACE TEMPERATURE AND NDVI: A CASE STUDY OF DEHRADUN, INDIA

Varinder Saini*[1] and Reet Kamal Tiwari[1]
[1]Dept. of Civil Engineering, Indian Institute of Technology Ropar, Nangal Road, Rupnagar 140001, Punjab, India
Email: varinder126@gmail.com (*corresponding author); reetkamal@gmail.com

KEY WORDS: Urbanization, NDVI, Land surface temperature (LST), Vegetation, Urban areas, Remote Sensing

ABSTRACT: One of the significant environmental consequences of urbanization is reduction in vegetation cover and formation of urban heat island effect. The present research utilized Landsat data from 1998 to 2017 to study the spatio-temporal pattern of NDVI and land surface temperature (LST) in Dehradun - capital of the newly formed state of Uttarakhand, which experienced rapid urbanization since 2000. LST has been calculated from thermal data of Landsat TM/TIRS using emissivity derived from NDVI images. The spatio-temporal pattern of LST indicates that urban/built-up area has increased over two decades and has higher temperature than the surrounding vegetated areas. LST statistics show that there has been a rise of 3.5 degrees in the minimum and 4.9 degrees in the maximum temperature in the 19 years. Urbanization leads to increase in the built-up areas which inturn get heated up as compared to the surrounding areas leading to urban heat island effect. In addition, correlation has been attempted between NDVI and LST. The results show an obvious negative correlation between the two *i.e.* the NDVI values are low or even negative where LST is high and vice-versa.

1. INTRODUCTION

The world is undergoing the largest wave of urban growth in history. At present, more than half of the world's population is living in urban areas such as towns and cities, and it is expected that by 2030 this number will increase to about 5 billion (UNFPA). United Nations Population Fund (UNFPA) also predicted that much of this urbanization will take place in Africa and Asia, bringing huge social, economic and environmental transformations. Sterling and Ducharne, (2008) pointed out that approximately 40% of the Earth's surface is covered by anthropogenic land-cover and that the natural vegetation-dominated landscapes have been replaced by impervious surfaces.

Dehradun district ranks 2nd in terms of population and is the most urbanized district of Uttarakhand with 55% of the population living in urban areas. It has a high population density with 549 persons per sq km. Decadal population growth rate (32.33% from 2001-2011) of the district is much above the state average of 18.81% (DCHD, 2011). It has been estimated that population of Dehradun will grow at a rate of 3% per annum till 2019 (UUDP, 2007). This may be attributed to the fact that this city has emerged as an important business, educational and cultural destination in north India after becoming the capital of newly formed Uttarakhand state since the year 2000 (Singh *et al.*, 2013). In addition to this, Dehradun is a rapidly growing trade centre and is also famous as a tourism destination among the masses. Therefore, as the industry and tourism sectors grow, the growth of service sector also accelerates, accentuating population growth. To accommodate this growing population, urban areas will further increase thus taking a toll on the natural resources especially vegetation and agricultural land. The study presented here gives an insight into the changing vegetation and temperature patterns of Dehradun city and its surrounding areas due to increase in urbanization. To achieve this, the NDVI and land surface temperature (LST) images derived from Landsat TM/OLI-TIRS have been used.

NDVI is generally considered as a good indicator of vegetation vigour, density and health in an area and is the most commonly used vegetation index. NDVI is a numerical indicator that uses red and NIR bands of remote sensing data to assess whether the land cover includes live, green vegetation or not. The index, first conceived by Rouse *et al.* (1973), is based on the absorption of light by vegetation in the red band and its reflectance in near-infrared band. The formula for measuring NDVI is given in equation 3. The value of NDVI ranges from -1 to +1 where -1 corresponds to pixel having no vegetation and +1 to pixel with dense vegetation cover. Literature indicates a consistent correlation between NDVI and vegetation biomass and dynamics in a number of ecosystems globally (Running, 1990; Myneni and Williams, 1994). Further, extensive exploration of NDVI's relationship with climatic variables has helped in making future predictions possible (Gong and Shi, 2003; Wand *et al.*, 2003). Therefore, the NDVI represents the first useful

tool which can amalgamate vegetation, ecosystem, climate and environment and perform studies at large spatial and temporal scales (Pettorelli *et al.,* 2005).

The thermal infrared (TIR) band of sensors onboard Landsat satellite is useful for calculating the LST. LST has been defined as the temperature of the interface between the earth's surface and its closest atmosphere and thus it is a crucial variable to understand the land-atmospheric interactions. LST is also one of the most important parameters in the physical processes of surface energy and water balance at local through global scales (Brunsell and Gillies, 2003; Anderson *et al*., 2008; Zhang *et al*., 2008; Kustas and Anderson, 2009; Karneilli *et al*., 2010). LST is most frequently used in a number of studies including evapo-transpiration, climate change, hydrological cycle, vegetation monitoring, urban climate and environmental studies such as urban heat island studies (Bastiaanssen *et al.,* 1998; Arnfield, 2003; Weng *et al*., 2004; Yuan and Bauer, 2007; Kalma *et al.,* 2008; Weng, 2009; Liu and Zhang, 2011). The correlation between LST and vegetation indices, such as NDVI, has been extensively documented in the literature. Mallick *et al*. (2008) examined the relationship between the NDVI and the LST using Landsat 7 ETM+ data and found reasonably strong relationship between the two variables. The land-cover category of dense vegetation (forest) and high dense built-up showed the highest (R^2= -0.752) and the lowest (R^2= -0.394) correlation in Delhi (India). A number of similar studies showing a negative correlation between LST and NDVI have been attempted (Yuan and Bauer, 2007; Yue *et al*., 2007; Imhoff *et al*., 2010; Molnar, 2016).

In the present study, NDVI based emissivity method has been used to derive LST (Valor and Caselles, 1996; Sobrino and Raissouni, 2000). It is based on a statistical relationship between the NDVI derived from the VNIR bands and the land surface emissivity (LSE) in the TIR bands (Li *et al.,* 2013). The amount of vegetation determines LST by the latent heat flux from the surface to atmosphere via evapo-transpiration. Areas with high NDVI are usually found to have lower LSTs (Yuan and Bauer, 2007). Therefore, the present research has been conducted to study the spatio-temporal pattern of LST and NDVI in Dehradun city and surrounding areas and study their correlation.

2. STUDY AREA AND DATA USED

Dehradun district is located in the Shiwalik range of Himalayas on the western border of the state of Uttarakhand covering an area of 3088 sq km (Figure 1). Dehradun city is located in the southern part of the Dehradun district between latitudes 30°15' and 30°25' N and longitudes 78°00' and 78°15' E. Since the urban areas exceed the old boundaries of the city, therefore, for the present study, Dehradun city (shown as black outline in Figure 1(c)) and the surrounding areas have been considered. The green triangles in the FCC show the location of the field temperature points (discussed in section III(B)). Three Landsat images, have been used for this study. The detail of the data used is given in Table 1.

Table I: Specifications of Landsat data used in the study.

Satellite/ Sensor	Acquisition Date(s)	Bands Used	Spectral Wavelength (µm)	Spatial Resolution (m)
Landsat-5/ TM	30 Dec. 1998 25 Dec. 2008	Red (Band 3)	0.63-0.69	30
		Near-infrared (Band 4)	0.76-0.90	30
		Thermal infrared (Band 6)	10.40-12.50	120*
Landsat-8/ OLI-TIRS	1 Feb. 2017	Red (Band 4)	0.64-0.67	30
		Near-infrared (Band 5)	0.85-0.88	30
		Thermal infrared (Band 10)	10.60-11.19	100*

**TIR/TIRS bands are acquired at 120/100 m resolutions, but are resampled to 30 m in delivered data product.*

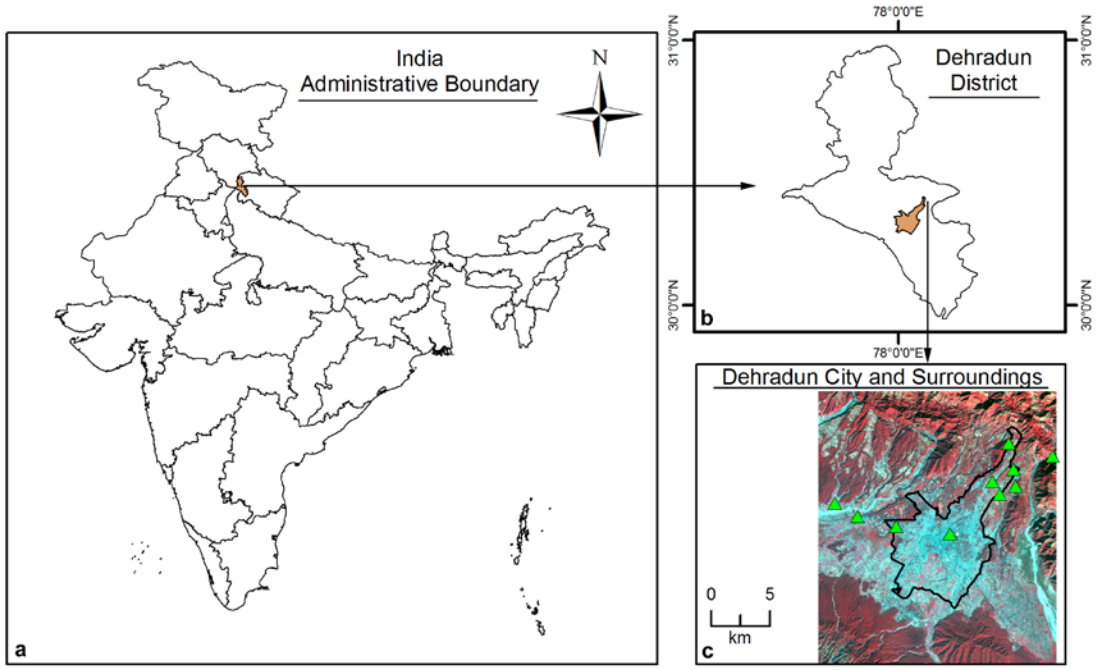

Figure 1. Location map of Dehradun district (b), and city (black outline in (c)). The green triangles in the standard FCC (R = NIR; G = Red; B = Green) of 2008 denote sample locations for field temperature measurements.

3. METHODOLOGY

The methodology comprises of both satellite data based calculations and field based measurements. For deriving LST and NDVI from satellite data, multi-temporal multi-sensor images (from year 1998 to 2017) acquired in red, near-infrared (NIR) and thermal infrared (TIR) bands of Landsat TM/OLI-TIRS sensors have been used. The digital number (DN) values of pixels in red and NIR bands have been converted to top-of-atmospheric reflectance and later into NDVI. In order to have an estimate of the temporal variations of NDVI over the years, images have been density sliced into three classes as defined in the study conducted by Gangopadhyay *et al.* (2006):

i) **Non-vegetated Area:** Pixels having NDVI values below 0.2. It includes water bodies, dry river beds, shadow, barren lands, built-up areas (both residential and industrial) and other such areas having no vegetation.
ii) **Sparse Vegetation:** Pixels having NDVI values between 0.2 and 0.5. It includes areas covered with shrubs, herbs, small trees etc.
iii) **Moderate to Dense Vegetation:** Pixels having NDVI values above 0.5. It includes natural forests/dense vegetation and similar areas.

DN of the thermal bands has been converted to radiant temperature and later into LST for whole of Dehradun city and surrounding areas. Since emissivity, which depends upon surface characteristics, plays an important role in calculation of LST, it has been suitably taken into account to refine the computed LST values. NDVI images have been used to calculate emissivity in this study ((5) and (6)). The temperature data collected during field survey using an infrared thermometer have been used to verify the LST derived from thermal remote sensing images.

3.1 LST Determination from Remote Sensing Images

Deriving LST from satellite sensor based TIR measurements require radiometric calibration, emissivity and atmospheric corrections (Vidal, 1991; Li *et al.*, 1993). A number of different approaches have been proposed to derive LST from TIR bands, using a variety of methods to calculate emissivity and atmospheric effects as inputs to the computation model of LST (Hook *et al.*, 1992; Kerr *et al.*, 1992; Kealy and Hook, 1993; Wan and Dozier, 1996; Pozo *et al.*, 1997; Wan and Li, 1997; Gillispie *et al.*, 1998; Qin *et al.*, 2001; Jiménez-Muñoz and Sobrino, 2003).

Landsat TM has only one thermal band so it has a limitation that the well known and accepted methods of split window algorithm (Sobrino *et al*., 2001) or temperature/emissivity separation (TES) method (Gillispie *et al*., 1998) cannot be applied. Landsat OLI-TIRS had two bands - band 10 and 11- but band 11 showed striping so here only band 10 has been used. Therefore, an NDVI based single window algorithm for deriving land surface emissivity (LSE) has been used in the present study. Out of the different approaches given in the literature (Van de griend and Owe, 1993; Valor and Caselles, 1996; Sobrino and Raissouni, 2000), a modification of the NDVI Thresholds Method ($NDVI^{THM}$) (Van de griend and Owe, 1993) has been used here. The following steps are followed to retrieve LST from thermal images and NDVI images.

a. Calculation of radiance images: The raw digital number (DN) values of TM have been converted to radiance using the formula given by Chander *et al*., (2009):

$$L^* = \frac{(L_{max} - L_{min})DN + L_{min}}{DN_{max}} \quad (1)$$

where L^* is the spectral radiance received at the sensor; L_{min} and L_{max} are the minimum and the maximum spectral radiance for the sensor respectively; DN_{max} is the maximum DN. For TIRS, the following formula is used (USGS, 2014):

$$L^* = M_L \times DN + A_L \quad (2)$$

where M_L is band specific multiplicative rescaling factor and A_L is the band specific additive rescaling factor from the metadata.

b. Calculation of radiant temperature: The radiance images derived from thermal bands have been used to calculate radiant temperature using the following formula (Chander *et al*., 2009):

$$T_r = \frac{K2}{ln\left(\frac{K1}{L^*} + 1\right)} \quad (3)$$

where T_r = radiant temperature (in Kelvin); *K1* and *K2* = pre-launched calibration constants 1 and 2 respectively (W/ (m^2 sr μm)); L^* = spectral radiance.

c. Creation of NDVI images: NDVI is based on vegetation reflectance and has been calculated using data acquired in Red and NIR band of the Landsat satellite. Atmospherically corrected bands have been used as the NDVI values derived from these may be more representative of the natural surfaces than derived from DN values. NDVI images have been calculated using the formula given by Rouse *et al*., (1973):

$$NDVI = \frac{\text{NIR} - \text{Red}}{\text{NIR} + \text{Red}} \quad (4)$$

where *Red* and *NIR* are the spectral reflectance of vegetation in the red band and the near infrared band respectively.

d. Calculation of emissivity: Sobrino *et al*., (2004) considered 49 soil spectra included in the ASTER spectral library and obtained the following expression for deriving LSE from pixels having proportion of both soil and vegetation:

$$\varepsilon = 0.004\ p_v + 0.986 \quad (5)$$

where p_v = vegetation proportion and can be derived from NDVI image according to the equation given by Carlson and Ripley, (1997):

$$p_v = \left[\frac{NDVI - NDVI_{min}}{NDVI_{max} - NDVI_{min}}\right]^2 \quad (6)$$

where $NDVI_{max}$ = 0.5 and $NDVI_{min}$ = 0.2. The values 0.5 and 0.2 are used for scenes which have the presence of bare

soil and vegetation respectively. It has been reported that this equation is the most suitable if there is a presence of bare soil and vegetation in a pixel, which is the case in the study area.

e. Calculation of LST: The outputs derived from (3) and (5) have been then used as inputs to calculate the LST using the following formula (Weng *et al.,* 2004):

$$LST = \frac{T_r}{1+\left(\frac{\lambda T_r}{\rho}\right)\ln\varepsilon} \quad (7)$$

where λ = central wavelength (in µm) of the Landsat thermal band; $\rho = 1.438 * 10^{-2}$ m K.

The NDVI and LST images thus derived have been used to study the spatio-temporal pattern.

3.2Field based temperature measurements

A handheld infrared thermometer was used to estimate the ground temperature at different surfaces. This instrument operates in a wide range of temperature (-20 to 320 °C) and spectral coverage (8-14 µm). A laser pointer makes it easy to point on a particular object from a distance. The measurements have been recorded from a distance of approximately 1m.

A total of 10 sample locations (Figure 1(c)) have been covered to record temperature during field survey conducted in the first week of February 2017 so as to corroborate as close as possible with the satellite overpass. The sample locations correspond to areas having different surface conditions such as vegetated areas (green as well as dry vegetation); barren areas; built-up areas; water bodies among others. The temperature data collected from these sample locations have been later used to validate the LSTs derived from thermal images.

4. RESULTS AND DISCUSSION

4.1 Spatio-temporal analysis of NDVI

In order to have an estimate of the temporal variations of NDVI over the years, all the three images have been density sliced into three classes as described in Section 3 above. Figure 2(a-c) shows the density sliced images for the years 1998, 2008 and 2017. It can be seen that in 2017 image non-vegetated area has increased to a large extent as compared to 1998. The built-up area has now exceeded the limits of the city especially on eastern and southern sides. In 1998, the point marked as 1 (Rajpur and nearby areas) in Figure 2(a-c) is having moderate to dense vegetation but in 2008 it changed to sparse vegetation and by 2017, most of it has changed to non-vegetated area. This is because, earlier this part used to be under natural vegetation and agricultural land, but with increasing population new residential complexes have been set up here. Moreover, Rajpur falls enroute Mussorie - a very popular tourist destination among masses - which has led to construction of numerous hotels and restaurants all along the Rajpur - Mussorie road.

Similarly, the point marked 2 (Banjarewala) in the southern part of the city in Figure 2(a-c) used to be an agricultural area in the past, but to accommodate the increasing population almost whole of this area has been now converted to built-up area. The point marked as 3 seem to show a trend that moderate to dense vegetation has increased in 2017 (Figure 2c) as compared to 2008 (Figure 2b). The area is agricultural land where rabi crop is sown in October/November. Since the 2008 image is from December, so the crop plants are still young and do not give much reflectance in NIR region. On the other hand, 2017 image is from February, when the crops are tall and green and thus give high reflectance in NIR region and resulting high NDVI values.

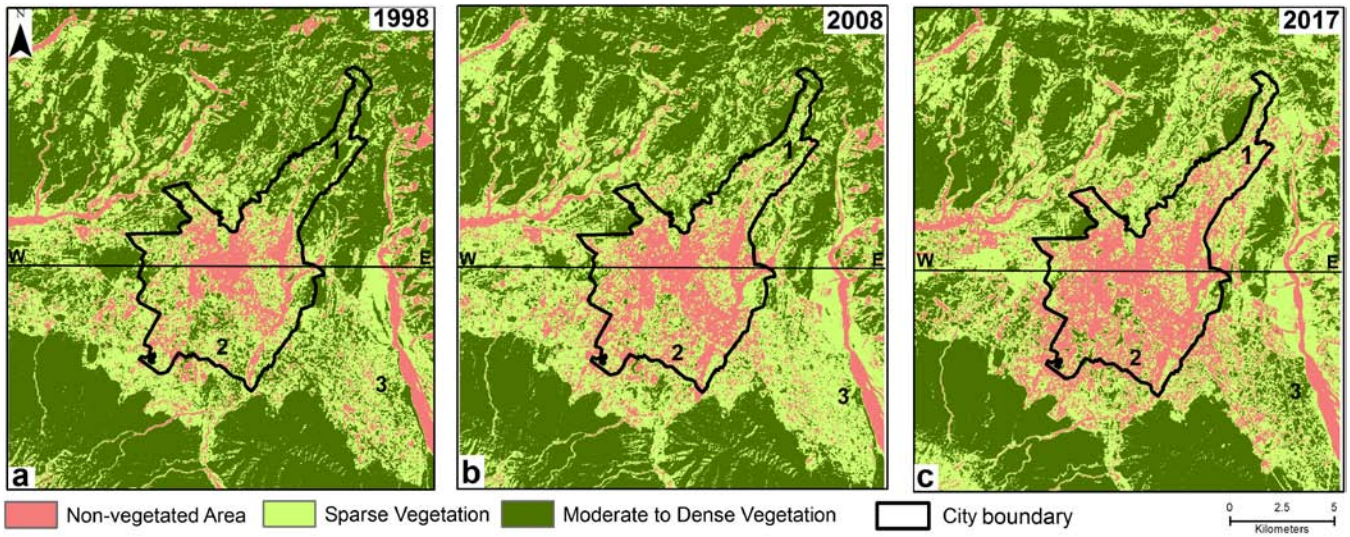

Figure 2. Density sliced NDVI images generated for the period 1998- 2017. Note: how the spatial distribution of non-vegetated area and vegetation has changed over the period. Black line represents W–E profiles along which NDVI profiles have been generated for studying correlation in Figure 5 below.

4.2 Spatio-temporal analysis of LST

The spatial variation of LST has been studied over a period of 19 years from 1998 to 2017. Figure 3(a-c) shows the spatial distribution of LST for the years 1998, 2008 and 2017. The high temperature areas have been shown in the shades of brown and correspond to built-up areas, open surfaces or barren hill slopes, dried river beds etc. whereas the cooler areas are depicted by the shades of green and correspond to water bodies, vegetation and agricultural land. Upon analysis, it has been observed that the minimum and maximum temperature in the study area has been increasing since 1998. There has been a rise of 3.5 degrees in the minimum and 4.9 degrees in the maximum temperature in the 19 years. Urbanization leads to increase in the built-up areas which inturn get heated up as compared to the surrounding areas leading to urban heat island effect. This is apparent from the visual appreciation of the 1998 and 2017 image contrasts.

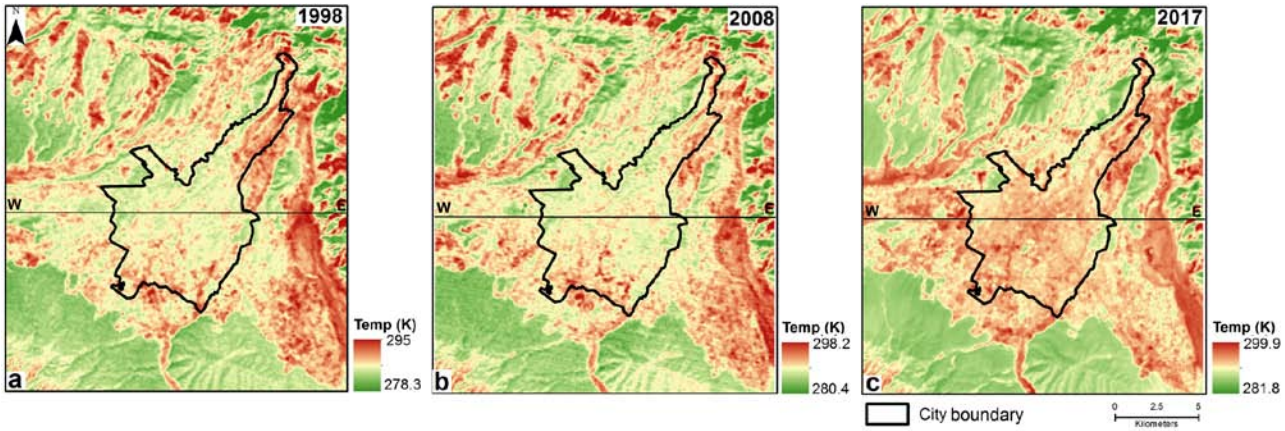

Figure 3. Spatial variation of LST for the years a) 1998, b) 2008, and c) 2017. All the values are in Kelvin. Black line represents W–E profiles along which LST profiles have been generated for studying correlation in Figure 5 below.

4.3 Validation of remote sensing derived LST

The field temperature measurements were planned to be as near as possible to the date of satellite overpass. The Landsat-8 data is of 1st February 2017 and the field temperature measurements were also taken between 1st - 4th February 2017. Therefore, the temperatures measured in field using the handheld infrared thermometer have been

compared with the corresponding temperature values obtained from the LST image of 2017. The locations (latitude/longitude) of the points from where temperature data have been used for field validation are shown in Table 2. It can be seen that the data have been collected from points located over various land use/land cover (LULC) classes such as built-up areas, vegetated areas, water bodies, barren/open areas, for better representation. The field observed temperature values and the corresponding LST values from all the three year images have been shown in the form of bar graphs (Figure 4).

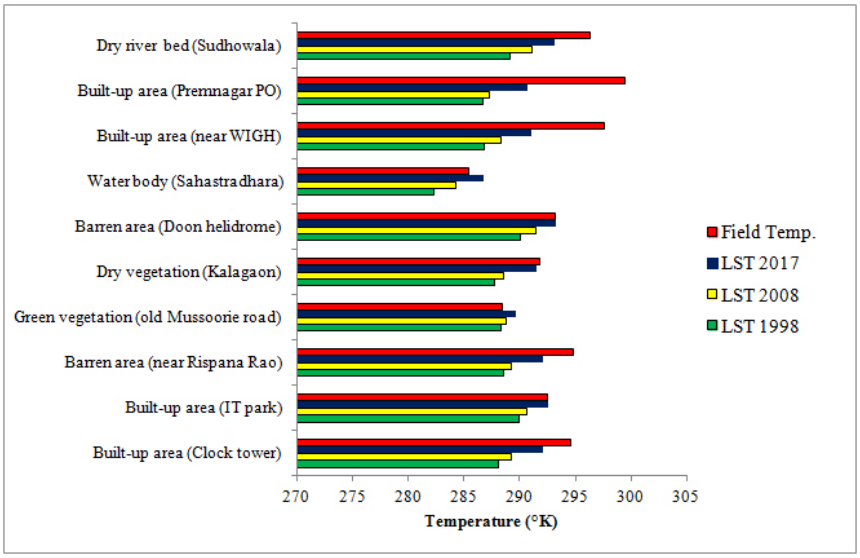

Figure 4. Bar graphs showing comparison of temperatures for the years 1998, 2008 and 2017 over different sample locations. Thermal image derived temperatures for the year 2017 have been validated through field temperature measurements as both have been obtained at almost the same dates. *For details, refer text.*

Table 2: Sample locations and their names used for validation of lst with field temperatures.

S. No	Land Cover/location	Latitude (DMS)	Longitude (DMS)	LST (°K)			Field Temp. (°K)
				1998	2008	2017	
1	Built up area (Clock tower)	30° 19' 28	78° 02' 31	288.1	289.2	292.1	294.6
2	Built up area (IT park)	30° 21' 21	78° 05' 07	289.9	290.6	292.6	292.5
3	Barren area (near Rispana Rao)	30° 21' 56	78° 04' 42	288.6	289.2	292.1	294.8
4	Green vegetation (old Mussoorie road)	30° 23' 43	78° 05' 30	288.3	288.8	289.7	288.4
5	Dry vegetation (Kalagaon)	30° 21' 45	78° 05' 57	287.8	288.6	291.5	291.8
6	Barren area (Doon helidrome)	30° 22' 32	78° 05' 48	290.1	291.5	293.3	293.2
7	Water body (Sahastradhara)	30° 23' 10	78° 07' 52	282.3	284.3	286.8	285.4
8	Built up area (near WIGH)	30° 20' 20	77° 59' 37	286.8	288.3	291.0	297.6
9	Built up area (Premnagar PO)	30° 20' 09	77° 57' 33	286.7	287.3	290.7	299.5
10	Dry river bed (Sudhowala)	30° 20' 43	77° 56' 20	289.1	291.1	293.1	296.3

After analysis, it may be seen that the temperature from field and LST values is comparable for all the LULC classes except the two built-up areas (Premnagar PO and near WIGH). The reason for this mismatch may be attributed to the fact that the satellite image derived temperature is at about 10 am (local time of satellite overpass) while the field temperature measurements of these points were taken at around 1 pm. The increased temperature may be due to heating up of the area in the afternoon.

4.4 Correlation between NDVI and LST

High temperature areas also generally tend to have lower NDVI values. This aspect has also been corroborated from the analysis of the relationship between LST and NDVI. There is an apparent correlation between NDVI and LST from the visual interpretation of NDVI and LST contrasts. In the LST images, the LST values of non-vegetated areas (built-up, barren, dried river beds) are higher than those obtained for areas pertaining to water bodies and vegetation including agricultural land (Figures 3(a-c)). The values are opposite in the NDVI images (Figures 2(a-c)). In order to study the variance of NDVI and LST, the pixel values of NDVI and LST are derived based on W–E profiles (shown as black line in Figures 2(a-c) and 3(a-c)).The profiles (Figure 5) show that the peaks of the LST are usually the areas where there are built-up areas, while the troughs are mostly where the water bodies and vegetation are found. The peaks of NDVI appear at vegetated areas including agricultural lands. Thus, NDVI and LST show an obvious negative correlation. In other words, the NDVI values are low (or even negative) where LST is high and vice-versa.

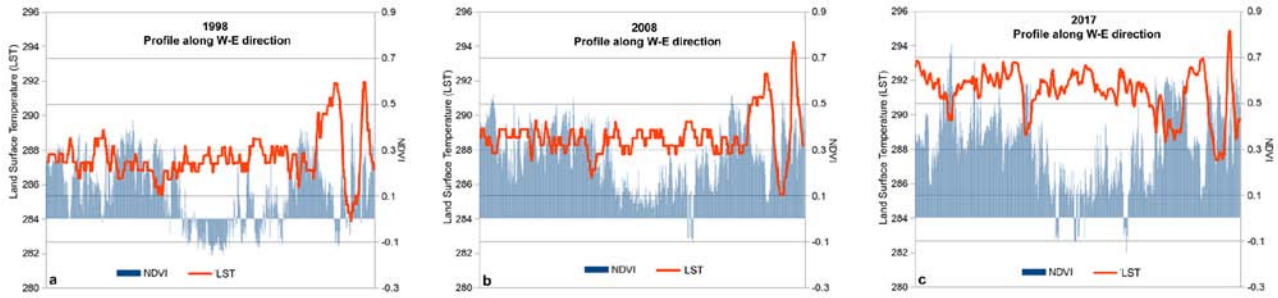

Figure 5. Correlation curves of NDVI and LST images of the years (a) 1998, (b) 2008, and (c) 2017. Profiles are taken along the black lines to show the LST and NDVI variance along the W-E profiles shown in Figures 2 and 3 above.

5. CONCLUSION

The study highlights the change in the vegetation over the last two decades in Dehradun city and the surrounding areas. An integrated approach of remote sensing has been successfully employed for determining NDVI and LST changes using satellite images. The changes are mainly negative which can directly be related to the rapid urbanization in the study area. The impact of urbanization has been large in the last decade due to the change in the socio-economic conditions of this area. The decrease in the vegetation is accompanied with the rise in minimum and maximum LST of the area. These changes also point out to the rapid urbanization of Dehradun city and the surrounding areas. This type of study can thus be used to monitor the urban sprawl and other vegetation related phenomena.

ACKNOWLEDGMENT

The authors thank the USGS (http://glovis.usgs.gov/) for providing the Landsat data used in this work free of cost through the internet.

REFERENCES

[1] Anderson, M.C., Norman, J.M., Kustas, W.P., Houborg, R., Starks, P.J., Agam, N., 2008. A thermal-based remote sensing technique for routine mapping of land-surface carbon, water and energy fluxes from field to regional scales. Remote Sensing of Environment, 112(12), pp. 4227–4241.

[2] Arnfield, A.J. 2003. Two decades of urban climate research: a review of turbulence, exchanges of energy and water, and the urban heat island. *International Journal of Climatology*, 23(1), pp. 1–26.

[3] Bastiaanssen, W.G.M., Menenti, M., Feddes, R.A., Holtslag, A.A.M., 1998. A remote sensing surface energy balance algorithm for land (SEBAL). 1. Formulation. *Journal of Hydrology*, 212, pp. 198–212.

[4] Brunsell, N.A., Gillies, R.R., 2003. Length scale analysis of surface energy fluxes derived from remote sensing. Journal of Hydrometeorology, 4, pp. 1212–1219.

[5] Carlson, T.N., Ripley, D.A. 1997. On the relation between NDVI, fractional vegetation cover, and leaf area index. *Remote Sensing of Environment*, 62(3), pp. 241–252.

[6] Chander, G., Markham, B.L., Helder, D.L. 2009. Summary of current radiometric calibration coefficients for Landsat MSS, TM, ETM+, and EO-1 ALI sensors. *Remote Sensing of Environment,* 113(5), pp. 893-903.
[7] DCDH, 2011. District Census Handbook Dehradun- Village and Town Wise Primary Census Abstract (PCA), Directorate of Census Operations, Uttarakhand, India, Series -06, Part XII-B, Retrieved February 12, 2017 from http://www.censusindia.gov.in/2011census/dchb/0505_PART_B_DCHB_DEHRADUN.pdf
[8] Gangopadhyay, P.K., Lahiri-Dutt, K., Saha, K. 2006. Application of remote sensing to identify coalfires in the Raniganj coalbelt, India. *International Journal of Applied Earth Observation and Geoinformation,* 8(3), pp. 188–195.
[9] Gillespie, A.R., Rokugawa, S., Matsunaga, T., Cothern, J.S., Hook, S., Kahle, A.B., 1998. A temperature and emissivity separation algorithm for Advanced Spaceborne Thermal Emission and Reflection Radiometer (ASTER) images. *IEEE Transactions on Geoscience and Remote Sensing,* 36(4), pp. 1113–1126.
[10] Gong, D.Y., Shi, P.J., 2003. Northern hemispheric NDVI variations associated with large-scale climate indices in spring. International Journal of Remote Sensing, 24(12), pp. 2559–2566.
[11] Hansen, J., Ruedy, R., Sato, M., Lo, K., 2010. Global surface temperature change. *Reviews of Geophysics,* 48, RG4004.
[12] Hook, S.J., Gabell, A.R., Green, A.A., Kealy, P.S., 1992. A comparison of techniques for extracting emissivity information from thermal infrared data for geologic studies. *Remote Sensing Environment,* 42(2), pp. 123–135.
[13] Imhoff, M.L., Zhang, P., Wolfe, R.E., Bounoua, L., 2010. Remote sensing of the urban heat island effect across biomes in the continental USA. *Remote Sensing of Environment,* 114(3) pp. 504–513.
[14] Jiménez-Muñoz, J.C., Sobrino, J.A. 2003. A generalized single-channel method for retrieving land surface temperature from remote sensing data. *Journal of Geophysical Research,* 108(D22), pp. 4688–4695.
[15] Karnieli, A. *et al*. 2010. Use of NDVI and land surface temperature for drought assessment: merits and limitations, Journal of Climatology, 23(3), pp. 618-633.
[16] Kealy, P.S., Hook, S.J., 1993. Separating temperature and emissivity in thermal infrared multispectral scanner data: Implications for recovering land surface temperatures. *IEEE Transactions on Geoscience and Remote Sensing,* 31(6), pp. 1155–1164.
[17] Kerr, Y.H., Lagouarde, J.P., Imbernon, J. 1992. Accurate land surface temperature retrieval from AVHRR data with use of an improved split window algorithm. *Remote Sensing of Environment,* 41(2-3), pp. 197–209.
[18] Kustas, W., Anderson, M. 2009. Advances in thermal infrared remote sensing for land surface modeling. Agricultural and Forest Meteorology, 149(12), pp. 2071–2081.
[19] Li, Z.-L., Becker, F., 1993. Feasibility of land surface temperature and emissivity determination from AVHRR data. *Remote Sensing of Environment,* 43(1), pp. 67–85.
[20] Li, Z.-L., Wu, H., Wang, N., Qiu, S., Sobrino, J.A., Wan, Z., *et al.,* 2013. Review article: Land surface emissivity retrieval from satellite data. *International Journal of Remote Sensing,* 34(9-10), pp. 3084-3127.
[21] Liu, L., Zhang, Y., 2011. Urban Heat Island Analysis Using the Landsat TM Data and ASTER Data: A Case Study in Hong Kong. *Journal of Remote Sensing,* 3(7), pp. 1535–1552.
[22] Mallick, J. Kant, Y., Bharat, B.D., 2008. Estimation of land surface temperature over Delhi using Landsat-7 ETM+. Journal of Indian Geophysical Union, 12(3), pp. 131-140.
[23] Molnar, G., 2016. Analysis of land surface temperature and NDVI distribution for Budapest using Landsat 7 ETM+ data. Acta Climatologica et Chorologica, 49-50, pp. 49-61.
[24] Myneni, R.B., Williams, D.L., 1994. On the relationship between FAPAR and NDVI. Remote Sensing of Environment, 49, pp. 200-211.
[25] Pettorelli, N., Vik, J.O., Mysterud, A., Gaillard, J., Tucker, C.J., Stenseth, N.C., 2005. Using the satellite-derived NDVI to assess ecological responses to environmental change. Trends in Ecology and Evolution, 20 pp. 503–510.
[26] Pozo Vazquez, D., Olmo Reyes, F.J., Alados Arboledas, L., 1997. A comparative study of algorithms for estimating land surface temperature from AVHRR data. *Remote Sensing of Environment,* 62(3), pp. 215–222.
[27] Qin, Z., Karnieli, A., Berliner, P. 2001. A mono-window algorithm for retrieving land surface temperature from Landsat TM data and its application to the Israel-Egypt border region. *International Journal of Remote Sensing,* 22(18), pp. 3719–3746.
[28] Rouse, J.W., Haas, R.H., Schell, J.A., Deering, D.W., 1973. Monitoring vegetation systems in the Great Plains with ERTS. Proceedings of 3rd ERTS Symposium, NASA SP-351 I, pp. 309–317.
[29] Running, S.W., 1990. Estimating primary productivity by combining remote sensing with ecosystem simulation. In: Remote Sensing of Biosphere Functioning, edited by Hobbs, R.J., Mooney, H.A., Springer-Verlag, Minnesota, pp. 65–86.
[30] Singh, O., Arya, P., Chaudhary, B.S., 2013. On rising temperature trends at Dehradun in Doon valley of Uttarakhand, India. Journal of Earth System Science, 122(3), pp. 613–622.

[31] Sobrino, J. A., Raissouni, N., Li, Z.-L., 2001. A comparative study of land surface emissivity retrieval from NOAA data. *Remote Sensing of Environment*, 75(2), pp. 256 – 266.
[32] Sobrino, J.A., Jimenez-Munoz, J.C., Paolini, L., 2004. Land surface temperature retrieval from Landsat TM 5. *Remote Sensing of Environment*, 90(4), pp. 434 – 440.
[33] Sobrino, J.A., Raissouni, N., 2000. Toward remote sensing methods for land cover dynamic monitoring: application to Morocco. *International Journal of Remote Sensing*, 21(2), pp. 353–366.
[34] Sterling, S., Ducharne, A., 2008. Comprehensive data set of global land cover change for land surface model applications. Global Biogeochemical Cycles, 22(3), pp. GB3017.
[35] UNFPA (United Nations Population Fund). Urbanization. Retrieved February 12, 2017, from http://www.unfpa.org/urbanization
[36] USGS, 2014. Using the USGS Landsat 8 product. Retrieved December 11, 2014 from https://landsat.usgs.gov/using-usgs-landsat-8-product
[37] UUDP (Uttaranchal Urban Development Project) 2007. Urban Development Department, Government of Uttaranchal, Dehradun, India, p. 65. Retrieved February 11, 2017 from http://s3.amazonaws.com/zanran_storage/www.adb.org/ContentPages/4506197.pdf
[38] Valor, E., Caselles, V. 1996. Mapping land surface emissivity from NDVI: application to European, African, and South American areas. *Remote Sensing of Environment*, 57(3), pp. 167–184.
[39] Van de Griend, A. A., Owe, M. 1993. On the relationship between thermal emissivity and the normalized difference vegetation index for natural surfaces. *International Journal of Remote Sensing*, 14(6), pp. 1119–1131.
[40] Vidal, A., 1991. Atmospheric and emissivity correction of land surface temperature measured from satellite using ground measurements or satellite data. *International Journal of Remote Sensing*, 12(12), pp. 2449–2460.
[41] Wan, Z., Dozier, J. 1996. A generalized split-window algorithm for retrieving land-surface temperature from space. *IEEE Transactions on Geoscience and Remote Sensing*, 34(4), pp. 892–905.
[42] Wan, Z., Li, Z.-L., 1997. A physics-based algorithm for retrieving land-surface emissivity and temperature from EOS/MODIS data. *IEEE Transactions on Geoscience and Remote Sensing*, 35(4), pp. 980–996.
[43] Wang, J., Rich, P.M., Price, K.P., 2003. Temporal responses of NDVI to precipitation and temperature in the central Great Plains, USA. International Journal of Remote Sensing, 24, pp. 2345–2364.
[44] Weng, Q., 2009. Thermal infrared remote sensing for urban climate and environmental studies: methods, applications, and trends. *ISPRS Journal of Photogrammetry and Remote Sensing*, 64(4), pp. 335–344.
[45] Weng, Q., Lu, D., Schubring, J. 2004. Estimation of land surface temperature–vegetation abundance relationship for urban heat island studies. *Remote Sensing of Environment*, 89(4), pp. 467-483.
[46] Yuan, F., Bauer, M.E., 2007. Comparison of impervious surface area and normalized difference vegetation index as indicators of surface urban heat island effects in Landsat imagery. *Remote Sensing of Environment*, 106(3), pp. 375-386.
[47] Yue, W., Xu, J., Tan W., Xu, L., 2007. The relationship between land surface temperature and NDVI with remote sensing: application to Shanghai Landsat 7 ETM+ data. *International Journal of Remote Sensing*, 128(15), pp. 3205-3226.
[48] Zhang, R., Tian, J., Su, H., Sun, X., Chen, S., Xia, J. 2008. Two improvements of an operational two-layer model for terrestrial surface heat flux retrieval. Sensors, 8(10), pp. 6165–6187.